
Language-Unlocked ViT (LUViT): Empowering Self-Supervised Vision Transformers with LLMs

Selim Kuzucu¹ * **Muhammad Ferjad Naeem²** **Anna Kukleva¹**
Federico Tombari² **Bernt Schiele¹**

¹Max Planck Institute for Informatics, SIC ²Google

Abstract

The integration of Large Language Model (LLMs) blocks with Vision Transformers (ViTs) holds immense promise for vision-only tasks by leveraging the rich semantic knowledge and reasoning capabilities of LLMs. However, a fundamental challenge lies in the inherent modality mismatch between text-centric pretraining of LLMs and vision-centric training of ViTs. Direct fusion often fails to fully exploit the LLM’s potential and suffers from unstable finetuning. As a result, LLM blocks are kept frozen while only the vision components are learned. As a remedy to these challenges, we introduce Language-Unlocked Vision Transformers (LUViT), a novel approach that bridges this modality mismatch through a synergistic pre-training strategy. LUViT co-adapts a ViT backbone and an LLM fusion block by (1) employing Masked Auto-Encoding (MAE) to pre-train the ViT for richer visual representations, and (2) concurrently training Low-Rank Adaptation (LoRA) layers within the LLM block using the MAE objective. This joint optimization guides the ViT to produce LLM-aligned features and the LLM to effectively interpret visual information. We demonstrate through extensive experiments that LUViT significantly improves performance on various downstream vision tasks, showcasing a more effective and efficient pathway to harness LLM knowledge for visual understanding.

1 Introduction

The remarkable success of Large Language Models (LLMs) [Brown et al., 2020, Touvron et al., 2023a] has revolutionized natural language processing, demonstrating advanced capabilities in understanding, generation, and reasoning. This success has led to significant interest in extending their power to other modalities, particularly vision, impacting the field of Vision-Language Models (VLMs) [Radford et al., 2021, Alayrac et al., 2022, Tschannen et al., 2025]. A promising direction within VLMs involves directly integrating powerful pre-trained LLM components with Vision Transformer (ViT) [Dosovitskiy et al., 2020] backbones, aiming to fuse visual models with the extensive semantic knowledge and reasoning abilities learned by LLMs from vast textual corpora.

However, these applications of LLM for vision explore them in a generative framework, limiting their application to discriminative computer vision tasks. Pioneering works like LM4Vision [Pang et al., 2023] have explored fusing ViT features with terminal blocks of LLMs while learning a computer vision task, hinting at the potential benefits. Regardless, a critical hurdle persists: the alignment of representations originating from different modalities. LLMs are pre-trained exclusively on text, optimizing their internal representations for linguistic structures and concepts. Similarly, ViTs learn visual features optimized for tasks like image recognition. Simply injecting visual features into a text-centric LLM block often results in suboptimal alignment [Liang et al., 2022], where the LLM

*Correspondence to skuzucu@mpi-inf.mpg.de

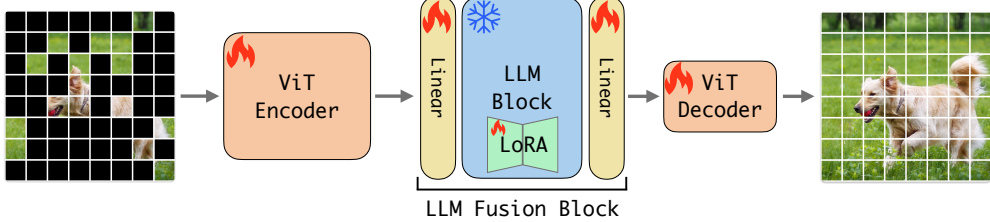


Figure 1: Architecture diagram of our **Language-Unlocked Vision Transformer (LUViT)**. Input image patches are processed by the ViT Encoder. The resulting visual features are then passed through an LLM Fusion Block (comprising linear projections and an LLM transformer block adapted with LoRA). For MAE pre-training, a lightweight decoder reconstructs masked patches. For fine-tuning, the decoder is removed, and a task-specific head is added.

struggles to effectively ground its textual knowledge in the visual domain. Furthermore, adapting the large LLM component to the visual modality by joint fine-tuning can be computationally prohibitive and risks catastrophic forgetting or training instabilities [Pang et al., 2023, Lai et al., 2024].

To address these challenges, we introduce **Language-Unlocked Vision Transformers (LUViT)**, a novel framework designed to foster a more profound and efficient synergy between ViTs and LLMs for discriminative vision tasks. Our core idea is a two-fold strategy:

1. **Enhanced Visual Representation Learning:** We pre-train the ViT backbone using Masked Auto-Encoding (MAE) [He et al., 2022]. This self-supervised objective encourages the ViT to learn richer, more context-aware visual representations that we hypothesize are more informative for an LLM.
2. **Efficient LLM Adaptation and Modality Bridging:** Simultaneously, we adapt the fused LLM block (e.g., from LLaMA) using Low-Rank Adaptation (LoRA) [Hu et al., 2022]. Crucially, these LoRA layers are trained *jointly* with the MAE pre-training of the ViT, using the same MAE reconstruction loss. This joint optimization allows the LLM to efficiently learn to interpret the evolving visual features, effectively translating its vast semantic knowledge to the visual domain without requiring full fine-tuning of the LLM.

This synergistic pre-training process is key: the ViT learns to produce “LLM-friendly” visual features, while the LLM (via LoRA) learns to “understand” these visual features, thereby bridging the modality mismatch from both ends. Our contributions are four-fold:

- We propose LUViT, a novel architecture and pre-training strategy that co-adapts a ViT and an LLM block through joint MAE-based self-supervision and LoRA-based LLM adaptation, effectively mitigating the alignment issue between representations of different modalities.
- We demonstrate that this concurrent optimization of LoRA layers within the LLM during MAE pre-training enables efficient and stable adaptation of the LLM, allowing it to effectively leverage its textual knowledge for visual understanding.
- We show through extensive experiments on benchmark computer vision tasks that LUViT significantly outperforms existing approaches that employ more direct fusion strategies, establishing a new state-of-the-art for unlocking LLM capabilities in vision models.
- We provide intriguing analyses regarding the attention entropies of LUViT and how it achieves stronger performance through improved background robustness.

2 Background and Related Work

Self-supervised learning. Self-supervised learning (SSL) has emerged as a powerful paradigm for leveraging readily available unlabeled data. SSL methods have achieved widespread success in the broader machine learning community, starting with earlier contrastive approaches [Chen et al., 2020a, He et al., 2020], achieving new frontiers in representation learning otherwise unreachable with full-supervised techniques. More recently, SSL approaches have powered foundation models in a wide range of domains, from NLP [Touvron et al., 2023a,b, Devlin et al., 2019] to vision [Caron et al., 2021, Grill et al., 2020, Naeem et al., 2024].

Masked image modeling. Masked image modeling is an established example of self-supervised learning methods for computer vision, initially pioneered by stacked denoising autoencoders [Vincent et al., 2010]. Motivated by the success of masked language modeling approach of BERT [Devlin et al., 2019], a plethora of follow-up works proposed novel self-supervised masked image modeling techniques [Chen et al., 2020b, Bao et al., 2021, Zhou et al., 2021, Dosovitskiy et al., 2020]. Among these works, Masked Auto-Encoders (MAE) [He et al., 2022] stand out with their accelerated pretraining approach consisting of a heavyweight encoder observing only a small fraction of image patches and a lightweight decoder reconstructing the original image features. MAE has established itself as a strong approach not only for global image recognition but also for more challenging fine-grained visual recognition tasks, such as object detection [Li et al., 2022a].

Large language models for visual tasks. Large language models (LLMs) are utilized in unison with visual encoders in numerous different multi-modal architecture settings. The most common branch of these works involve using the LLMs as the *text decoders* of large vision-language models [Li et al., 2022b, 2023, Liu et al., 2023, Chen et al., 2024a,b, Alayrac et al., 2022], where they are preceded by visual encoders. In these works, encoder-processed visual tokens are simply projected to the text decoder [Li et al., 2022b, Liu et al., 2023] or fused through additional cross-modal layers [Alayrac et al., 2022].

All of the aforementioned works demonstrate that LLMs can process vision-originating data, given that they are processed by a separate visual encoder [Liu et al., 2023, Li et al., 2022b] or trained jointly from scratch on vast amounts of data in multiple stages [Diao et al., 2024, Wang et al., 2025, Luo et al., 2024]. Our work is inspired by the success of the aforementioned approaches, while differentiating in several key aspects. Namely, our goal is to effectively leverage LLM transformer blocks and Self-Supervised Learning (SSL) for improving the performance of vision transformers [Dosovitskiy et al., 2020], without relying on language-aligned visual encoders (e.g. CLIP [Radford et al., 2021]) or requiring language inputs.

Using frozen LLM blocks for visual tasks. Closest to our work are the works directly employing frozen pretrained LLM blocks with vision transformers [Pang et al., 2023, Lai et al., 2024, Bai et al., 2025]. Among these, Pang et al. [2023] is the pioneering work that showed that using frozen LLaMA 1 [Touvron et al., 2023a] blocks on top of vision transformer encoders can provide strong performance gains on a wide range of vision tasks. However, Pang et al. [2023] did not aim to achieve SOTA performance on visual recognition but rather show the relative performance improvement on a test bench on a variety of vision tasks. Following up from [Pang et al., 2023], Bai et al. [2025] aimed to provide a more detailed explanation for the improved performance of vision transformers under the presence of LLM blocks, showing that the LLM blocks improve the gradient coherence during training.

In this work, we combine the powers of self-supervised learning, the initial explorations of Pang et al. [2023], and LoRA adaptations together to achieve drastically improved downstream performance, differing from previous works. Supported with our experiments, our work provides stronger recipes for achieving stellar visual recognition performance while effectively leveraging the LLM blocks.

3 LUViT: Language-Unlocked Vision Transformers

While LM4Vision [Pang et al., 2023] demonstrated the potential of fusing Vision Transformers (ViTs) with the terminal block of a Large Language Model (LLM), the direct introduction of this transformer block introduces a modality mismatch due to the LLM’s text-centric pre-training and Vision Transformer’s visual processing. To address this, we propose a twofold strategy. First, we introduce Self-Supervised Learning (SSL) using Masked Auto-Encoding (MAE) during the pre-training of the ViT backbone. This step aims to better align visual representations with the language modality. Second, to adapt the LLM component (e.g., LLaMA), which has been pre-trained solely on text, we incorporate Low-Rank Adaptation (LoRA). This allows the LLM to efficiently translate its extensive semantic knowledge, learned from billion-scale textual data, to the visual domain, thereby improving performance on target computer vision tasks.

LUViT: Language-Unlocked Vision Transformer

We introduce Language-Unlocked Vision Transformers (LUViT), with the aim of effectively bridging the representation alignment issue between vision and language representations when using language

trained transformer blocks in vision transformers. The core intuition is to enable a synergistic co-adaptation: the ViT learns to produce visual features amenable to language processing, while the LLM block learns to interpret these visual features, all within a unified pre-training framework.

Our LUViT architecture (illustrated in Figure 1) comprises three main components:

1. **Vision Transformer (ViT) Encoder (\mathbf{M}_{Enc}):** Following [Dosovitskiy et al., 2020], the standard ViT maps input patches x into latent visual representations $z_v = \mathbf{M}_{Enc}(x)$.
2. **LLM Fusion Block ($\mathbf{M}_{LLM}^{\text{fuse}}$):** This module integrates a pre-trained LLM transformer block (e.g., from LLaMA [Touvron et al., 2023a]) into pipeline to enrich the visual features z_v . To manage differing hidden dimensions and facilitate adaptation, z_v is first projected by a linear layer \mathbf{M}_L^1 , then processed by the LLM block \mathbf{M}_{LLM} , and finally projected back by \mathbf{M}_L^2 . Thus, the enhanced latent features are $z'_v = \mathbf{M}_L^2 \cdot \mathbf{M}_{LLM} \cdot \mathbf{M}_L^1(z_v)$. We denote this entire compound mapping as $\mathbf{M}_{LLM}^{\text{fuse}}(z_v) \rightarrow z'_v$.
3. **Lightweight MAE Decoder (\mathbf{M}_{Dec}):** For self-supervised pre-training, a shallow transformer decoder, similar to [He et al., 2022], takes the enhanced latent features z'_v from visible patches and reconstructs the original masked image patches x' .

The complete pre-training pipeline for an input image x can thus be expressed as:

$$x' = \mathbf{M}_{Dec}(\mathbf{M}_{LLM}^{\text{fuse}}(\mathbf{M}_{Enc}(x_{\text{vis}})), x_{\text{mask_ids}}), \quad (1)$$

where x_{vis} represents visible (unmasked) patches fed to the encoder, and $x_{\text{mask_ids}}$ represents information about the masked patches required by the decoder for reconstruction (e.g., their positional embeddings).

Synergistic Pre-training for Modality Alignment

The core component of LUViT is its pre-training strategy, designed to address the modality mismatch through self-supervised pretraining. This involves concurrently training the ViT via Masked Auto-Encoding (MAE) and adapting the LLM fusion block using LoRA.

Self-Supervised Visual Representation Learning via MAE

Intuition. Standard ViT training (e.g., on ImageNet) learns features optimized for classification but these features often fail to capture deeper semantics required for other computer vision tasks [He et al., 2022]. However, self-supervised pretrained backbones learn more generic features often directly usable across a plethora of computer vision tasks [Oquab et al., 2023, He et al., 2022]. We utilize Masked Auto-Encoding (MAE) [He et al., 2022] as the self-supervision framework owing to its recent success in learning robust features and its efficiency [He et al., 2022, Tschannen et al., 2025]. MAE learns holistic and context-aware representations by reconstructing heavily masked inputs. When learned together with a LLM block, we hypothesize that such representations are inherently richer and more compatible with the high-level understanding capabilities of LLM block.

Mechanism. We follow the standard MAE pre-training strategy proposed by [He et al., 2022]. An input image x is divided into N non-overlapping patches. A high percentage (e.g., 75%) of these patches are randomly masked out. Only the visible patches x_{vis} are processed by the ViT encoder \mathbf{M}_{Enc} and subsequently by the LLM fusion block $\mathbf{M}_{LLM}^{\text{fuse}}$. The lightweight decoder \mathbf{M}_{Dec} takes the output from the LLM block and reconstructs the original pixels of the masked patches from the enhanced latent representations z'_v and the positional embeddings of all patches. The learning objective minimizes the Mean Squared Error (MSE) between the reconstructed and original masked patches. This process trains the ViT backbone \mathbf{M}_{Enc} .

Efficient LLM Adaptation with Low-Rank Adaptation (LoRA)

Intuition. Pre-trained LLMs possess vast world knowledge and complex reasoning abilities encoded in their weights. Fine-tuning the entire LLM for a vision task is computationally prohibitive and risks catastrophic forgetting of its semantic understanding capabilities that we want to utilize for visual understanding. LoRA [Hu et al., 2022] offers a parameter-efficient solution, allowing us to "steer" the LLM's knowledge towards the visual domain by training only a small number of additional

parameters. It also allows for stable finetuning of the LLM block without the risk of the larger LLM block collapsing the training signal.

Mechanism. We inject LoRA layers into the query (W_q) and value (W_v) projection matrices of the LLM block \mathbf{M}_{LLM} . For a pre-trained weight matrix $W_0 \in \mathbb{R}^{d \times k}$, its update is represented by a low-rank decomposition $W_0 + \Delta W = W_0 + BA$, where $B \in \mathbb{R}^{d \times r}$, $A \in \mathbb{R}^{r \times k}$, and the rank $r \ll \min(d, k)$. Only A and B are trainable. The original LLM weights W_0 remain frozen keeping their pre-trained knowledge secure.

Joint Optimization: The Key to Modality Bridging

A critical aspect of our method is that the LoRA layers within $\mathbf{M}_{LLM}^{\text{fuse}}$ are trained *concurrently* with the ViT backbone during the MAE pre-training phase. The MAE reconstruction loss not only guides the ViT but also backpropagates through the LLM fusion block, updating the LoRA parameters. This joint optimization fosters a synergistic co-adaptation during learning, while the ViT (\mathbf{M}_{Enc}) learns to produce visual embeddings that are not only good for reconstruction but are also effectively processed and enhanced by the LLM block. The LLM block learns to interpret and refine these evolving visual embeddings via LoRA in \mathbf{M}_{LLM} , leveraging its pre-trained frozen textual knowledge to enhance them with richer semantics relevant to the visual context.

This simultaneous learning process is crucial for bridging the modality mismatch, as it forces the two modalities to be jointly aligned rather than adapting one to a fixed representation of the other. The LLM is not just passively processing ViT features; it is actively being aligned to understand the visual world while the ViT learns to present this information in a more digestible format in the LLM space.

Architectural Adjustments for Cross-Modal LLM Processing

To further enhance the LLM block’s suitability for processing visual information, we incorporate specific architectural modifications, building upon insights from prior work [Pang et al., 2023, Lai et al., 2024]. **(1) Bidirectional Attention.** Standard LLMs often use causal attention masks, as the next token prediction objective should only attend to past information. However, visual information in an image does not possess inherent sequential causality in the same way. Thus, we replace the causal attention mechanism in the LLM block with bidirectional attention. This allows each visual token representation within the LLM block to attend to all other tokens, allowing a holistic understanding. **(2) Removal of Rotary Positional Embeddings (RoPE).** RoPE [Su et al., 2024], commonly used in LLMs like LLaMA, encodes absolute and relative positional information tailored for text sequences. Since our ViT backbone already incorporates learned positional embeddings for visual patches, and the nature of spatial relationships in images differs from sequential text, we remove RoPE from the LLM block. This simplifies the architecture, prevents the imposition of text-specific positional biases onto visual features, and ensures consistency with typical ViT designs that do not use RoPE.

Downstream Fine-tuning

After the MAE-based pre-training with joint LoRA adaptation, LUViT is fine-tuned for specific downstream computer vision tasks (e.g., image classification). For fine-tuning, we discard the MAE decoder (\mathbf{M}_{Dec}), and add a task-specific head (e.g., a linear classifier) on top of the output features z'_v . During fine-tuning, the ViT backbone, the linear projection layers \mathbf{M}_L^1 , \mathbf{M}_L^2 , and the LoRA parameters within the LLM block can be further trained. The original weights of the LLM block \mathbf{M}_{LLM} remain frozen, preserving its extensive learned knowledge while allowing targeted adaptation through LoRA. This strategy ensures efficient transfer of learned representations to downstream tasks.

4 Experiments

We now discuss our experiments and highlight the strengths of our Language-unlocked Vision Transformers (LUViT).

Datasets. For our image classification experiments, we utilize the Imagenet-1K training and validation splits [Deng et al., 2009]. In addition, we report evaluation results on several domain-shift benchmarks, namely Imagenet-C [Hendrycks and Dietterich, 2019], Imagenet-A [Hendrycks et al., 2021a], Imagenet-SK [Wang et al., 2019], Imagenet-V2 [Recht et al., 2019], and Imagenet-R [Hendrycks et al., 2021b]. Furthermore, we report additional results on Imagenet-9 benchmark [Xiao et al., 2020],

which measures the reliance of a model on background and foreground features. Among its splits, we choose the *mixed same* and the *mixed random*. In the former, backgrounds of images are randomly replaced with the background of another image of the same class, and in the latter the background is replaced with the background of an image of a completely random class. Finally, for our fine-grained visual recognition experiments, we use the MS COCO [Lin et al., 2014] object detection dataset. We report our results on the COCO validation set, following the previous works [Li et al., 2022a].

Pretraining. Our pre-training settings closely mirror that of the original MAE work He et al. [2022], including all of the hyperparameters related to the training (learning rate, batch size, masking ratio, *etc.*). We pre-train both vanilla MAE ViT baselines and our LUViT for a total of 800 epochs, following He et al. [2022]. For our LLM block, unless otherwise specified, we always utilize the 32nd transformer block of LLaMA 1 Touvron et al. [2023a], similarly with Pang et al. [2023]. As described earlier in Section 3, while the original LLM transformer weights are always kept frozen, we also integrate LoRA [Hu et al., 2022] to the query and value projection matrices, both of which have a rank of 16, only constituting a very minor fraction (0.3%) of the number of trainable parameters.

End-to-end Finetuning. For image classification, we perform finetuning for 100 epochs on both the baselines and our LUViT following the pre-training stage, while adhering to all of the hyperparameter settings and other training details presented in [He et al., 2022]. Analogously for fine-grained visual recognition, we also train for 100 epochs for both the baselines and LUViT following the pre-training stage, while adhering to all of the training settings in ViTDet [Li et al., 2022a]. From ViTDet, we utilize the simple feature pyramid [Lin et al., 2017] version with Mask R-CNN [He et al., 2017].

4.1 Image Classification

We evaluate LUViT on the challenging ImageNet-1K benchmark and its variants designed to test robustness to domain shifts (ImageNet-A, ImageNet-Sketch, ImageNet-V2, ImageNet-R) and common corruptions (ImageNet-C). The results, presented in Table 1, demonstrate the performance improvements of our proposed approach.

LUViT outperforms all baselines. Our LUViT/B model establishes a new state-of-the-art on ImageNet-1K among comparable methods, achieving 83.6% top-1 accuracy. This surpasses not only the supervised ViT/B baseline (80.6%) but also the prior LLM-augmented supervised model LM1+ViT/B* (81.7%) from [Pang et al., 2023]. More critically, LUViT outperforms the strong MAE-pretrained ViT/B baseline (83.2%), demonstrating the impact of our synergistic LLM integration beyond the standard MAE pretraining.

LUViT better Unlocks LLM Benefits. The MAE-pretrained ViT/B already provides a powerful visual backbone, outperforming the supervised LM1+ViT/B* (83.2% vs. 81.7% on IN-1K). However, LUViT consistently builds upon this strong foundation and achieves respectable improvements. The improvements of LUViT over the MAE-ViT baseline (e.g., +0.4% on IN-1K, +2.2% on IN-A, +0.8% on IN-SK) directly validate our hypothesis: concurrently training the LoRA-adapted LLM block during MAE pre-training enables the LLM to effectively process and enhance visual features. This joint optimization addresses the modality mismatch in an effective manner, allowing the LLM to contribute its semantic knowledge to the visual task, a benefit not realized by simply pre-training the ViT with MAE alone or even with extra learning capacity as shown in Section 4.3.

Enhanced Robustness and Generalization. The advantages of LUViT become even more pronounced on robustness benchmarks. On IN-A, a particularly challenging adversarial dataset, LUViT achieves a 2.2% absolute improvement over the MAE-ViT baseline, reaching 36.0%, with respectable gains also observed on IN-SK (+0.8%), IN-V2 (+0.7%), and IN-C (+0.5%). With these results, the superior performance over the MAE-pretrained ViT shows that our method of integrating and adapting the LLM component brings tangible benefits beyond self-supervised visual pre-training. Second, it shows substantial improvements on robustness benchmarks (especially IN-A). The results indicate that LUViT successfully leverages the LLM’s knowledge to achieve improved resilience against out-of-distribution samples which is particularly important for real-world vision systems. Third, by outperforming previous attempts at LLM-ViT fusion, like LM1+ViT/B* [Pang et al., 2023], LUViT demonstrates the importance of both a strong pre-training paradigm (MAE) and an efficient adaptation strategy (concurrent LoRA training) to reap the benefits of the LLM block.

Table 1: LUViT achieves state-of-the-art Top-1 accuracy (%) in frozen LLM augmented model setting on ImageNet-1K. We also demonstrate significantly enhanced robustness across its challenging variants (IN-A, IN-SK, IN-V2, IN-R, IN-C). LUViT consistently outperforms both supervised baselines and the strong MAE-pretrained ViT/B. * denotes numbers from Pang et al. [2023]. **Bold** indicates the best result, underline the second best.

Training	Model	IN-1K	IN-A	IN-SK	IN-V2	IN-R	IN-C
Supervised-Only	ViT/B*	80.6	23.4	31.9	—	43.5	60.2
	LM1+ViT/B*	81.7	26.9	33.2	—	44.3	62.1
MAE Pretrained	ViT/B	<u>83.2</u>	<u>33.8</u>	<u>36.0</u>	<u>72.5</u>	<u>50.1</u>	<u>62.9</u>
	LUViT/B (<i>Ours</i>)	83.6	36.0	36.8	73.2	50.2	63.4
		<u>+0.4</u>	<u>+2.2</u>	<u>+0.8</u>	<u>+0.7</u>	<u>+0.1</u>	<u>+0.5</u>

4.2 Fine-grained Visual Recognition

The results on MS COCO, presented in Table 2, demonstrate LUViT’s capability to enhance fine-grained visual recognition. Our LUViT/B model consistently outperforms the strong MAE ViT/B baseline across all reported metrics for both object detection and instance segmentation. Specifically, LUViT/B achieves a bounding box AP of **51.1**, an improvement of +0.5 AP over the MAE ViT/B. For instance segmentation, LUViT/B achieves a mask AP of **45.1** (+0.2 AP improvement), with notable gains in AP₅₀ (+0.6).

Table 2: Object detection and instance segmentation results on MS COCO [Lin et al., 2014] dataset. Bounding box AP values are for the detection results whereas the mask AP values are for the instance segmentation results. **Bold** denotes the best result for each setting.

Model	Bounding Box			Mask		
	AP	AP ₅₀	AP ₇₅	AP	AP ₅₀	AP ₇₅
MAE ViT/B	50.6	71.0	55.5	44.9	68.2	48.7
LUViT/B (<i>Ours</i>)	51.1	71.5	55.9	45.1	68.8	48.8
	<u>+0.5</u>	<u>+0.5</u>	<u>+0.4</u>	<u>+0.2</u>	<u>+0.6</u>	<u>+0.1</u>

4.3 Ablations

In this section we quantify the importance of the several building blocks of our approach: the LLM block, MAE objective and the importance of LoRA. We ablate over these components and report the results in Table 3 on ImageNet-1k and ImageNet-C datasets.

MAE Pre-training Forms a Strong Foundation. Consistent with prior research [He et al., 2022], MAE pre-training substantially boosts performance over supervised-only training. Comparing the supervised ViT/B (row a: 80.6% IN-1K, 60.5% IN-C) with the MAE-pretrained ViT/B (row c: 83.2% IN-1K, 62.9% IN-C) reveals significant performance improvements (+2.6% IN-1K, +2.4% IN-C). This confirms the importance of self-supervised learning for robust visual representations, which LUViT leverages as its starting point. Moreover, even when an LLM block is added, MAE pre-training remains beneficial: the MAE-pretrained LM1+ViT/B (row e: 83.1% IN-1K) outperforms its supervised counterpart (row b: 81.7% IN-1K).

LoRA Adaptation is Crucial for Unlocking LLM Benefits with MAE pre-training. Comparing row (c) and (e), we observe that the frozen LLM variant without any LoRA fine-tuning in row (e) (83.1% IN-1K, 62.9% IN-C) achieves onpar performance with the baseline MAE ViT of row (c) (row c: 83.2% IN-1K, 62.9% IN-C). This indicates that without adaptation, the LLM block does not benefit from the richer features coming from the MAE-pre-training. This is a contrast with Pang et al. [2023] where the improvements were possible without adaptation on a weaker baseline. However, when we introduce LoRA and adapt the LLM block, as in our full LUViT/B model (row h), performance significantly improves to **83.6%** on IN-1K and **63.4%** on IN-C. This is a clear improvement over both the MAE ViT/B baseline (row c) and the frozen LLM variant without LoRA (row e). This result confirms that LoRA-based adaptation is not just beneficial but *essential* for effectively bridging the modality mismatch and enabling the LLM to utilize the enhanced visual representations.

Table 3: Ablation analysis of LUViT components on ImageNet-1K and ImageNet-C confirms that LUViT design choices are essential to achieve the best performance. "Trainable Params" refers to parameters updated during the final fine-tuning stage (for MAE models, this includes the entire ViT, projections, and LoRA if present). ViT/B+MLP models are configured to match the trainable parameters of corresponding LLM-augmented models. * denotes numbers from Pang et al. [2023]. **Bold** indicates the best results.

Training	Model	Trainable Params.	IN-1K	IN-C
Supervised-Only	(a) ViT/B*	86.8M	80.6	60.5
	(b) ViT/B + LLaMA*	92.9M	81.7	62.1
MAE Pretrained	(c) ViT/B	86.8M	83.2	62.9
	(d) ViT/B + MLP-P	92.9M	83.1	63.1
	(e) ViT/B + LLaMA	92.9M	83.1	62.9
	(f) ViT/B + MLP-L	93.1M	83.3	63.0
	(h) LUViT/B (<i>Ours</i>)	93.1M	83.6 <i>+0.3</i>	63.4 <i>+0.3</i>

Table 4: Ablation analysis of the initialization of the LLM transformer on ImageNet-1K and ImageNet-C solidify the importance of language-pretrained representations. "Trainable Params" refers to parameters updated during the final fine-tuning stage, including the entire ViT, projections, and LoRA. "Random" denotes initializing the LLM block randomly whereas "Pretrained" denotes initializing the LLM block with language-pretrained weights. **Bold** indicates the best results.

LLM Init.	Model	Trainable Params.	IN-1K	IN-C
Random	ViT/B+LLaMA	93.1M	83.2	63.1
	LUViT/B (<i>Ours</i>)	93.1M	83.6 <i>+0.4</i>	63.4 <i>+0.3</i>

LUViT’s Gains are Not Merely from Increased Parameters. A critical question is whether LUViT’s improvements stem from our model design or from an increased number of trainable parameters introduced by the linear projections and LoRA. To investigate this, we create two stronger baselines, namely (1) **ViT/B+MLP-P (Proj. Match, row d)** and (2) **ViT/B+MLP-L (LoRA Match, row f)**. The former’s total trainable parameters (92.9M) match those of the LM1+ViT/B (row e), which includes the ViT and the trainable linear projections, whereas the latter’s total trainable parameters (93.1M) match those of our full LUViT/B model (row g), which includes the ViT, trainable projections, and trainable LoRA layers.

Comparing row (d) with row (e), the ViT/B+MLP (Proj. Match) performs on-par on both IN-C and IN-1K compared to the frozen LLM without LoRA. This suggests that at this parameter count, a generic MLP can be as effective as an unadapted LLM block. However, the crucial comparison is between our full LUViT/B model (row h) and its parameter-matched MLP counterpart (row f). LUViT/B achieves **83.6%** on IN-1K and **63.4%** on IN-C, outperforming ViT/B+MLP (LoRA Match) (row f: 83.3% IN-1K, 63.0% IN-C) by +0.3% on IN-1K and +0.4% on IN-C.

Pretrained LLM representations are Crucial for the Downstream Gains. To further investigate the role of the language-pretrained representations in the LLM block, we consider a randomly initialized LLaMA 1 block as another baseline instead of the language-pretrained weights in LUViT in Table 4. To ensure a fairer comparison, we follow the exact same architectural design, including the LoRA layers and linear projections of the full LUViT. Here, observe a similar pattern: The full LUViT with original LLaMA 1 weights outperforms the model with randomly initialized LLaMA 1 by +0.4% on IN-1K and 0.3% on IN-C.

These results further quantify that the improvements of LUViT are not simply due to additional training capacity but a direct consequence of our design choices and the knowledge adapted from the frozen LLM block.

5 On The Background Robustness of LUViT

In this section, we establish an intriguing connection between the background robustness and the improved performance by our LUViT models, after analyzing the attention entropy patterns. Previously, Pang et al. [2023] attempted to explain the effectiveness of using frozen LLM layers in vision tasks with the *information filtering hypothesis*. Particularly, Pang et al. [2023] hypothesized that the frozen LLM block could be acting as a filter, where it amplifies the final contributions of the informative tokens. However, despite their intriguing observations regarding the information filtering hypothesis, Pang et al. [2023] could not provide detailed discussions on the attention patterns, as they found the attention weights to be too noisy to provide insightful conclusions.

LUViT Exhibits More Focused Attention Patterns. As our work flourishes in the same spirit as LM4Vision [Pang et al., 2023] while improving it, we follow up from their initial explorations and analyze the attention entropies of both the MAE ViT/B baseline and our LUViT/B, thereby decrypting the previously under-explored attention patterns of ViTs utilizing LLM blocks. In particular, we quantify the attention entropies through taking the post-softmax entropy of each row of the attention matrix, where each row corresponds to a spatial location on the feature map. Formally, denoting the input as $X \in \mathbb{R}^{T \times d}$, and the query and key projection matrices as $W_Q \in \mathbb{R}^{d \times d_k}$, $W_K \in \mathbb{R}^{d \times d_k}$, the post-softmax attention matrix with its row-wise entropies are given by:

$$A = \text{softmax} \left[\frac{W_Q \cdot W_K^T}{\sqrt{d}} \right], \quad \mathcal{H}(A_i) = - \sum_{j=1}^T A_{i,j} \log(A_{i,j}). \quad (2)$$

We visualize the attention entropies using the Imagenet-S-300 dataset [Gao et al., 2022] in Figure 2. Here, we map each of the mask annotations in Imagenet-S-300 down to the resolution of our feature maps, and construct a binary mask for distinguishing the background versus foreground regions. Then, we average the entropies of tokens belonging to the foreground vs tokens belonging to the background for each image in Figure 2.

As we observe from Figure Figure 2, a lucid distinction between the average attention entropies for the background and foreground regions for our LUViT/B emerges, whereas the attention entropies are mostly the same for all regions of the MAE ViT/B baseline, regardless of whether they belong to a highly informative foreground region or not. This is a direct indication of the *focus* of the attention patterns for the informative foreground regions for LUViT, informative regions, resulting in LUViT relying more on foreground features while making predictions as shown qualitatively in Section A.1.

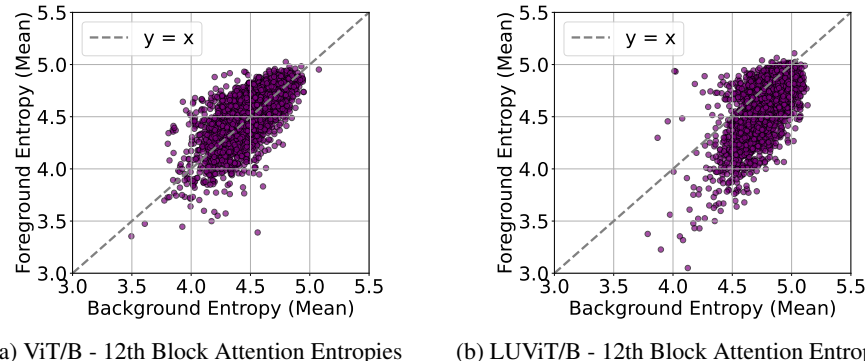


Figure 2: Comparison of the image-level average foreground attention entropies vs the image-level average background attention entropies of (a) MAE ViT/B baseline and (b) our LUViT/B model. Each point in the plots corresponds to an image on Imagenet-S-300 dataset [Gao et al., 2022]. LUViT’s average attention entropies are higher for background regions compared to foreground regions for 83% of the images. However, ViT/B’s average attention entropies are higher for background regions compared to foreground regions for only 43% of the images.

LUViT is More Robust Against Adversarial Backgrounds. Inspired by these observations in the attention patterns, we then benchmark our LUViT against the MAE ViT/B baseline on the challenging Imagenet-9 benchmark, described in Section 4. Our results are presented in Table 5, where the performance on the unaltered original split is close for both, with the gains with LUViT drastically

Table 5: Top-1 accuracy results of MAE pretrained models on Imagenet-9 background spurious correlations benchmark. The final three columns highlight the accuracy gap between different splits. **Bold** denotes best results.

Model	Original	Same	Random	<i>Orig.-Same</i> ↓	<i>Orig.-Rand.</i> ↓	<i>Same-Rand.</i> ↓
MAE ViT/B	96.5	87.8	83.2	8.7	13.3	4.6
LUViT/B (Ours)	96.6	89.2	85.3	7.4	11.3	3.9
	+0.1	+1.4	+2.1	-1.3	-2.0	-0.7

increasing as the altered backgrounds get more challenging. In particular, for the *Mixed Random*, LUViT/B improves the performance by **+2.1**, with this improvement further increasing to **+1.4** for the *Mixed Same*. Along with the performance gap, the background accuracy gaps between the original and mixed splits is also significantly improved with LUViT/B.

6 Conclusion

In this work, we introduce Language-Unlocked Vision Transformers (LUViT), a training framework that brings the semantic knowledge learned by text-only pre-trained LLM blocks into discriminative vision models. Our core contribution lies in a synergistic pre-training strategy that co-adapts both modalities: we leverage Masked Auto-Encoding (MAE) to learn rich visual representations from the ViT, while concurrently training Low-Rank Adaptation (LoRA) layers within an LLM block using the same MAE objective. This joint optimization process is crucial, guiding the ViT to produce LLM-friendly features while simultaneously enabling the LLM to effectively enhance these visual features with its vast semantic knowledge. Our comprehensive experiments demonstrate LUViT’s efficacy. On image classification benchmarks, LUViT not only establishes a new state-of-the-art result in this setting but also shows greatly improved robustness to domain shifts. We show that while MAE pre-training provides a vital foundation, the LoRA-based adaptation of the LLM block, trained in tandem, is essential for unlocking performance gains. LUViT offers an effective pathway to harness the extensive knowledge of pre-trained LLMs for vision tasks.

Bibliography

Tom Brown, Benjamin Mann, Nick Ryder, Melanie Subbiah, Jared D Kaplan, Prafulla Dhariwal, Arvind Neelakantan, Pranav Shyam, Girish Sastry, Amanda Askell, Sandhini Agarwal, Ariel Herbert-Voss, Gretchen Krueger, Tom Henighan, Rewon Child, Aditya Ramesh, Daniel Ziegler, Jeffrey Wu, Clemens Winter, Chris Hesse, Mark Chen, Eric Sigler, Mateusz Litwin, Scott Gray, Benjamin Chess, Jack Clark, Christopher Berner, Sam McCandlish, Alec Radford, Ilya Sutskever, and Dario Amodei. Language models are few-shot learners. In H. Larochelle, M. Ranzato, R. Hadsell, M.F. Balcan, and H. Lin, editors, *Advances in Neural Information Processing Systems*, volume 33, pages 1877–1901. Curran Associates, Inc., 2020. URL https://proceedings.neurips.cc/paper_files/paper/2020/file/1457c0d6bfc4967418bfb8ac142f64a-Paper.pdf.

Hugo Touvron, Thibaut Lavril, Gautier Izacard, Xavier Martinet, Marie-Anne Lachaux, Timothée Lacroix, Baptiste Rozière, Naman Goyal, Eric Hambro, Faisal Azhar, et al. Llama: Open and efficient foundation language models. *arXiv preprint arXiv:2302.13971*, 2023a.

Alec Radford, Jong Wook Kim, Chris Hallacy, Aditya Ramesh, Gabriel Goh, Sandhini Agarwal, Girish Sastry, Amanda Askell, Pamela Mishkin, Jack Clark, et al. Learning transferable visual models from natural language supervision. In *International conference on machine learning*, pages 8748–8763. PMLR, 2021.

Jean-Baptiste Alayrac, Jeff Donahue, Pauline Luc, Antoine Miech, Iain Barr, Yana Hasson, Karel Lenc, Arthur Mensch, Katherine Millican, Malcolm Reynolds, et al. Flamingo: a visual language model for few-shot learning. *Advances in neural information processing systems*, 35:23716–23736, 2022.

Michael Tschannen, Alexey Gritsenko, Xiao Wang, Muhammad Ferjad Naeem, Ibrahim Alabdulmohsin, Nikhil Parthasarathy, Talfan Evans, Lucas Beyer, Ye Xia, Basil Mustafa, et al. Siglip 2:

Multilingual vision-language encoders with improved semantic understanding, localization, and dense features. *arXiv preprint arXiv:2502.14786*, 2025.

Alexey Dosovitskiy, Lucas Beyer, Alexander Kolesnikov, Dirk Weissenborn, Xiaohua Zhai, Thomas Unterthiner, Mostafa Dehghani, Matthias Minderer, Georg Heigold, Sylvain Gelly, et al. An image is worth 16x16 words: Transformers for image recognition at scale. *arXiv preprint arXiv:2010.11929*, 2020.

Ziqi Pang, Ziyang Xie, Yunze Man, and Yu-Xiong Wang. Frozen transformers in language models are effective visual encoder layers. *arXiv preprint arXiv:2310.12973*, 2023.

Victor Weixin Liang, Yuhui Zhang, Yongchan Kwon, Serena Yeung, and James Y Zou. Mind the gap: Understanding the modality gap in multi-modal contrastive representation learning. *Advances in Neural Information Processing Systems*, 35:17612–17625, 2022.

Zhixin Lai, Jing Wu, Suiyao Chen, Yucheng Zhou, and Naira Hovakimyan. Residual-based language models are free boosters for biomedical imaging tasks. In *Proceedings of the IEEE/CVF Conference on Computer Vision and Pattern Recognition*, pages 5086–5096, 2024.

Kaiming He, Xinlei Chen, Saining Xie, Yanghao Li, Piotr Dollár, and Ross Girshick. Masked autoencoders are scalable vision learners. In *Proceedings of the IEEE/CVF conference on computer vision and pattern recognition*, pages 16000–16009, 2022.

Edward J Hu, Yelong Shen, Phillip Wallis, Zeyuan Allen-Zhu, Yuanzhi Li, Shean Wang, Lu Wang, Weizhu Chen, et al. Lora: Low-rank adaptation of large language models. *ICLR*, 1(2):3, 2022.

Ting Chen, Simon Kornblith, Mohammad Norouzi, and Geoffrey Hinton. A simple framework for contrastive learning of visual representations. In *International conference on machine learning*, pages 1597–1607. PMLR, 2020a.

Kaiming He, Haoqi Fan, Yuxin Wu, Saining Xie, and Ross Girshick. Momentum contrast for unsupervised visual representation learning. In *Proceedings of the IEEE/CVF conference on computer vision and pattern recognition*, pages 9729–9738, 2020.

Hugo Touvron, Louis Martin, Kevin Stone, Peter Albert, Amjad Almahairi, Yasmine Babaei, Nikolay Bashlykov, Soumya Batra, Prajjwal Bhargava, Shruti Bhosale, et al. Llama 2: Open foundation and fine-tuned chat models. *arXiv preprint arXiv:2307.09288*, 2023b.

Jacob Devlin, Ming-Wei Chang, Kenton Lee, and Kristina Toutanova. Bert: Pre-training of deep bidirectional transformers for language understanding. In *Proceedings of the 2019 conference of the North American chapter of the association for computational linguistics: human language technologies, volume 1 (long and short papers)*, pages 4171–4186, 2019.

Mathilde Caron, Hugo Touvron, Ishan Misra, Hervé Jégou, Julien Mairal, Piotr Bojanowski, and Armand Joulin. Emerging properties in self-supervised vision transformers. In *Proceedings of the IEEE/CVF international conference on computer vision*, pages 9650–9660, 2021.

Jean-Bastien Grill, Florian Strub, Florent Altché, Corentin Tallec, Pierre Richemond, Elena Buchatskaya, Carl Doersch, Bernardo Avila Pires, Zhaohan Guo, Mohammad Gheshlaghi Azar, et al. Bootstrap your own latent-a new approach to self-supervised learning. *Advances in neural information processing systems*, 33:21271–21284, 2020.

Muhammad Ferjad Naeem, Yongqin Xian, Xiaohua Zhai, Lukas Hoyer, Luc Van Gool, and Federico Tombari. Silc: Improving vision language pretraining with self-distillation. In *European Conference on Computer Vision*, pages 38–55. Springer, 2024.

Pascal Vincent, Hugo Larochelle, Isabelle Lajoie, Yoshua Bengio, Pierre-Antoine Manzagol, and Léon Bottou. Stacked denoising autoencoders: Learning useful representations in a deep network with a local denoising criterion. *Journal of machine learning research*, 11(12), 2010.

Mark Chen, Alec Radford, Rewon Child, Jeffrey Wu, Heewoo Jun, David Luan, and Ilya Sutskever. Generative pretraining from pixels. In *International conference on machine learning*, pages 1691–1703. PMLR, 2020b.

Hangbo Bao, Li Dong, Songhao Piao, and Furu Wei. Beit: Bert pre-training of image transformers. *arXiv preprint arXiv:2106.08254*, 2021.

Jinghao Zhou, Chen Wei, Huiyu Wang, Wei Shen, Cihang Xie, Alan Yuille, and Tao Kong. ibot: Image bert pre-training with online tokenizer. *arXiv preprint arXiv:2111.07832*, 2021.

Yanghao Li, Hanzi Mao, Ross Girshick, and Kaiming He. Exploring plain vision transformer backbones for object detection. In *European conference on computer vision*, pages 280–296. Springer, 2022a.

Junnan Li, Dongxu Li, Caiming Xiong, and Steven Hoi. Blip: Bootstrapping language-image pre-training for unified vision-language understanding and generation. In *International conference on machine learning*, pages 12888–12900. PMLR, 2022b.

Junnan Li, Dongxu Li, Silvio Savarese, and Steven Hoi. Blip-2: Bootstrapping language-image pre-training with frozen image encoders and large language models. In *International conference on machine learning*, pages 19730–19742. PMLR, 2023.

Haotian Liu, Chunyuan Li, Qingyang Wu, and Yong Jae Lee. Visual instruction tuning. *Advances in neural information processing systems*, 36:34892–34916, 2023.

Zhe Chen, Weiyun Wang, Yue Cao, Yangzhou Liu, Zhangwei Gao, Erfei Cui, Jinguo Zhu, Shenglong Ye, Hao Tian, Zhaoyang Liu, et al. Expanding performance boundaries of open-source multimodal models with model, data, and test-time scaling. *arXiv preprint arXiv:2412.05271*, 2024a.

Zhe Chen, Jiannan Wu, Wenhai Wang, Weijie Su, Guo Chen, Sen Xing, Muyan Zhong, Qinglong Zhang, Xizhou Zhu, Lewei Lu, et al. Internvl: Scaling up vision foundation models and aligning for generic visual-linguistic tasks. In *Proceedings of the IEEE/CVF conference on computer vision and pattern recognition*, pages 24185–24198, 2024b.

Haiwen Diao, Yufeng Cui, Xiaotong Li, Yueze Wang, Huchuan Lu, and Xinlong Wang. Unveiling encoder-free vision-language models. *arXiv preprint arXiv:2406.11832*, 2024.

Han Wang, Yongjie Ye, Bingru Li, Yuxiang Nie, Jinghui Lu, Jingqun Tang, Yanjie Wang, and Can Huang. Vision as lora. *arXiv preprint arXiv:2503.20680*, 2025.

Gen Luo, Xue Yang, Wenhan Dou, Zhaokai Wang, Jiwen Liu, Jifeng Dai, Yu Qiao, and Xizhou Zhu. Mono-internvl: Pushing the boundaries of monolithic multimodal large language models with endogenous visual pre-training. *arXiv preprint arXiv:2410.08202*, 2024.

Lichen Bai, Zixuan Xiong, Hai Lin, Guangwei Xu, Xiangjin Xie, Ruijie Guo, Zhanhui Kang, Hai-Tao Zheng, and Hong-Gee Kim. Frozen language models are gradient coherence rectifiers in vision transformers. In *Proceedings of the AAAI Conference on Artificial Intelligence*, volume 39, pages 1817–1825, 2025.

Maxime Oquab, Timothée Darcet, Théo Moutakanni, Huy Vo, Marc Szafraniec, Vasil Khalidov, Pierre Fernandez, Daniel Haziza, Francisco Massa, Alaaeldin El-Nouby, et al. Dinov2: Learning robust visual features without supervision. *arXiv preprint arXiv:2304.07193*, 2023.

Jianlin Su, Murtadha Ahmed, Yu Lu, Shengfeng Pan, Wen Bo, and Yunfeng Liu. Roformer: Enhanced transformer with rotary position embedding. *Neurocomputing*, 568:127063, 2024.

Jia Deng, Wei Dong, Richard Socher, Li-Jia Li, Kai Li, and Li Fei-Fei. Imagenet: A large-scale hierarchical image database. In *2009 IEEE conference on computer vision and pattern recognition*, pages 248–255. Ieee, 2009.

Dan Hendrycks and Thomas Dietterich. Benchmarking neural network robustness to common corruptions and perturbations. *arXiv preprint arXiv:1903.12261*, 2019.

Dan Hendrycks, Kevin Zhao, Steven Basart, Jacob Steinhardt, and Dawn Song. Natural adversarial examples. In *Proceedings of the IEEE/CVF conference on computer vision and pattern recognition*, pages 15262–15271, 2021a.

Haohan Wang, Songwei Ge, Zachary Lipton, and Eric P Xing. Learning robust global representations by penalizing local predictive power. In *Advances in Neural Information Processing Systems*, pages 10506–10518, 2019.

Benjamin Recht, Rebecca Roelofs, Ludwig Schmidt, and Vaishaal Shankar. Do imagenet classifiers generalize to imagenet? In *International conference on machine learning*, pages 5389–5400. PMLR, 2019.

Dan Hendrycks, Steven Basart, Norman Mu, Saurav Kadavath, Frank Wang, Evan Dorundo, Rahul Desai, Tyler Zhu, Samyak Parajuli, Mike Guo, et al. The many faces of robustness: A critical analysis of out-of-distribution generalization. In *Proceedings of the IEEE/CVF international conference on computer vision*, pages 8340–8349, 2021b.

Kai Xiao, Logan Engstrom, Andrew Ilyas, and Aleksander Madry. Noise or signal: The role of image backgrounds in object recognition. *arXiv preprint arXiv:2006.09994*, 2020.

Tsung-Yi Lin, Michael Maire, Serge Belongie, James Hays, Pietro Perona, Deva Ramanan, Piotr Dollár, and C Lawrence Zitnick. Microsoft coco: Common objects in context. In *Computer vision-ECCV 2014: 13th European conference, zurich, Switzerland, September 6-12, 2014, proceedings, part v 13*, pages 740–755. Springer, 2014.

Tsung-Yi Lin, Piotr Dollár, Ross Girshick, Kaiming He, Bharath Hariharan, and Serge Belongie. Feature pyramid networks for object detection. In *Proceedings of the IEEE conference on computer vision and pattern recognition*, pages 2117–2125, 2017.

Kaiming He, Georgia Gkioxari, Piotr Dollár, and Ross Girshick. Mask r-cnn. In *Proceedings of the IEEE international conference on computer vision*, pages 2961–2969, 2017.

Shanghua Gao, Zhong-Yu Li, Ming-Hsuan Yang, Ming-Ming Cheng, Junwei Han, and Philip Torr. Large-scale unsupervised semantic segmentation. *IEEE transactions on pattern analysis and machine intelligence*, 45(6):7457–7476, 2022.

Yong Guo, David Stutz, and Bernt Schiele. Robustifying token attention for vision transformers. In *Proceedings of the IEEE/CVF International Conference on Computer Vision*, pages 17557–17568, 2023.

Zhisong Zhang, Yan Wang, Xinting Huang, Tianqing Fang, Hongming Zhang, Chenlong Deng, Shuaiyi Li, and Dong Yu. Attention entropy is a key factor: An analysis of parallel context encoding with full-attention-based pre-trained language models. *arXiv preprint arXiv:2412.16545*, 2024.

Shuangfei Zhai, Tatiana Likhomanenko, Eta Littwin, Dan Busbridge, Jason Ramapuram, Yizhe Zhang, Jiatao Gu, and Joshua M Susskind. Stabilizing transformer training by preventing attention entropy collapse. In *International Conference on Machine Learning*, pages 40770–40803. PMLR, 2023a.

David Picard. Torch. manual_seed (3407) is all you need: On the influence of random seeds in deep learning architectures for computer vision. *arXiv preprint arXiv:2109.08203*, 2021.

Hugo Touvron, Matthieu Cord, Matthijs Douze, Francisco Massa, Alexandre Sablayrolles, and Hervé Jégou. Training data-efficient image transformers & distillation through attention. In *International conference on machine learning*, pages 10347–10357. PMLR, 2021.

Jinlong Liu, Guoqing Jiang, Yunzhi Bai, Ting Chen, and Huayan Wang. Understanding why neural networks generalize well through gsnr of parameters. *arXiv preprint arXiv:2001.07384*, 2020.

Mateusz Michalkiewicz, Masoud Faraki, Xiang Yu, Manmohan Chandraker, and Mahsa Baktashmotlagh. Domain generalization guided by gradient signal to noise ratio of parameters. In *Proceedings of the IEEE/CVF International Conference on Computer Vision*, pages 6177–6188, 2023.

Rishabh Tiwari and Pradeep Shenoy. Overcoming simplicity bias in deep networks using a feature sieve. In *International Conference on Machine Learning*, pages 34330–34343. PMLR, 2023.

Geoffrey Hinton, Oriol Vinyals, and Jeff Dean. Distilling the knowledge in a neural network. *arXiv preprint arXiv:1503.02531*, 2015.

Haiwen Diao, Xiaotong Li, Yufeng Cui, Yueze Wang, Haoge Deng, Ting Pan, Wenxuan Wang, Huchuan Lu, and Xinlong Wang. Eeve2: Improved baselines for encoder-free vision-language models. *arXiv preprint arXiv:2502.06788*, 2025.

Rohan Bavishi, Erich Elsen, Curtis Hawthorne, Maxwell Nye, Augustus Odena, Arushi Somani, and Sagnak Tasırlar. Introducing our multimodal models, 2023. URL <https://www.adept.ai/blog/fuyu-8b>, 2, 2023.

Yangyi Chen, Xingyao Wang, Hao Peng, and Heng Ji. A single transformer for scalable vision-language modeling. *arXiv preprint arXiv:2407.06438*, 2024c.

Jiahui Yu, Zirui Wang, Vijay Vasudevan, Legg Yeung, Mojtaba Seyedhosseini, and Yonghui Wu. Coca: Contrastive captioners are image-text foundation models. *arXiv preprint arXiv:2205.01917*, 2022.

Bo Wan, Michael Tschannen, Yongqin Xian, Filip Pavetic, Ibrahim M Alabdulmohsin, Xiao Wang, André Susano Pinto, Andreas Steiner, Lucas Beyer, and Xiaohua Zhai. Locca: Visual pretraining with location-aware captioners. *Advances in Neural Information Processing Systems*, 37:116355–116387, 2024.

Xiaohua Zhai, Basil Mustafa, Alexander Kolesnikov, and Lucas Beyer. Sigmoid loss for language image pre-training. In *Proceedings of the IEEE/CVF international conference on computer vision*, pages 11975–11986, 2023b.

Jimmy Lei Ba, Jamie Ryan Kiros, and Geoffrey E Hinton. Layer normalization. *arXiv preprint arXiv:1607.06450*, 2016.

Yash Goyal, Tejas Khot, Douglas Summers-Stay, Dhruv Batra, and Devi Parikh. Making the v in vqa matter: Elevating the role of image understanding in visual question answering. In *Proceedings of the IEEE conference on computer vision and pattern recognition*, pages 6904–6913, 2017a.

Xinlei Chen, Hao Fang, Tsung-Yi Lin, Ramakrishna Vedantam, Saurabh Gupta, Piotr Dollár, and C Lawrence Zitnick. Microsoft coco captions: Data collection and evaluation server. *arXiv preprint arXiv:1504.00325*, 2015.

Ashish Vaswani, Noam Shazeer, Niki Parmar, Jakob Uszkoreit, Llion Jones, Aidan N Gomez, Łukasz Kaiser, and Illia Polosukhin. Attention is all you need. *Advances in neural information processing systems*, 30, 2017.

Ilya Loshchilov and Frank Hutter. Sgdr: Stochastic gradient descent with warm restarts. *arXiv preprint arXiv:1608.03983*, 2016.

Diederik P Kingma. Adam: A method for stochastic optimization. *arXiv preprint arXiv:1412.6980*, 2014.

Ilya Loshchilov and Frank Hutter. Decoupled weight decay regularization. *arXiv preprint arXiv:1711.05101*, 2017.

Priya Goyal, Piotr Dollár, Ross Girshick, Pieter Noordhuis, Lukasz Wesolowski, Aapo Kyrola, Andrew Tulloch, Yangqing Jia, and Kaiming He. Accurate, large minibatch sgd: Training imagenet in 1 hour. *arXiv preprint arXiv:1706.02677*, 2017b.

Kevin Clark, Minh-Thang Luong, Quoc V Le, and Christopher D Manning. Electra: Pre-training text encoders as discriminators rather than generators. *arXiv preprint arXiv:2003.10555*, 2020.

Christian Szegedy, Vincent Vanhoucke, Sergey Ioffe, Jon Shlens, and Zbigniew Wojna. Rethinking the inception architecture for computer vision. In *Proceedings of the IEEE conference on computer vision and pattern recognition*, pages 2818–2826, 2016.

Gao Huang, Yu Sun, Zhuang Liu, Daniel Sedra, and Kilian Q Weinberger. Deep networks with stochastic depth. In *Computer Vision–ECCV 2016: 14th European Conference, Amsterdam, The Netherlands, October 11–14, 2016, Proceedings, Part IV 14*, pages 646–661. Springer, 2016.

Hongyi Zhang, Moustapha Cisse, Yann N Dauphin, and David Lopez-Paz. mixup: Beyond empirical risk minimization. *arXiv preprint arXiv:1710.09412*, 2017.

Sangdoo Yun, Dongyoon Han, Seong Joon Oh, Sanghyuk Chun, Junsuk Choe, and Youngjoon Yoo. Cutmix: Regularization strategy to train strong classifiers with localizable features. In *Proceedings of the IEEE/CVF international conference on computer vision*, pages 6023–6032, 2019.

Ekin D Cubuk, Barret Zoph, Jonathon Shlens, and Quoc V Le. Randaugment: Practical automated data augmentation with a reduced search space. In *Proceedings of the IEEE/CVF conference on computer vision and pattern recognition workshops*, pages 702–703, 2020.

A Paszke. Pytorch: An imperative style, high-performance deep learning library. *arXiv preprint arXiv:1912.01703*, 2019.

Ze Liu, Yutong Lin, Yue Cao, Han Hu, Yixuan Wei, Zheng Zhang, Stephen Lin, and Baining Guo. Swin transformer: Hierarchical vision transformer using shifted windows. In *Proceedings of the IEEE/CVF international conference on computer vision*, pages 10012–10022, 2021.

Kai Chen, Jiaqi Wang, Jiangmiao Pang, Yuhang Cao, Yu Xiong, Xiaoxiao Li, Shuyang Sun, Wansen Feng, Ziwei Liu, Jiarui Xu, et al. Mmdetection: Open mmlab detection toolbox and benchmark. *arXiv preprint arXiv:1906.07155*, 2019.

Kaiming He, Xiangyu Zhang, Shaoqing Ren, and Jian Sun. Deep residual learning for image recognition. In *Proceedings of the IEEE conference on computer vision and pattern recognition*, pages 770–778, 2016.

Nicolas Carion, Francisco Massa, Gabriel Synnaeve, Nicolas Usunier, Alexander Kirillov, and Sergey Zagoruyko. End-to-end object detection with transformers. In *European conference on computer vision*, pages 213–229. Springer, 2020.

Alexandre Lacoste, Alexandra Luccioni, Victor Schmidt, and Thomas Dandres. Quantifying the carbon emissions of machine learning. *arXiv preprint arXiv:1910.09700*, 2019.

Supplementary Material

Contents

1	Introduction	1
2	Background and Related Work	2
3	LUViT: Language-Unlocked Vision Transformers	3
4	Experiments	5
4.1	Image Classification	6
4.2	Fine-grained Visual Recognition	7
4.3	Ablations	7
5	On The Background Robustness of LUViT	9
6	Conclusion	10
	Bibliography	10

A More Visualizations with Attention Entropies	16
A.1 Image-level Attention Entropy Visualizations	16
A.2 Additional Attention Entropy Scatter Plots	18
B Additional Experimental Results	19
B.1 Error Bars for Imagenet-1K Experiments	19
B.2 Adapting the LLM Under Supervised-only Training	19
B.3 Additional Results on Imagenet-Segmentation Benchmark	20
C Further Discussions on Related Works	21
C.1 Information Filtering Hypothesis	21
C.2 Pretrained LLM Layers and Gradient Coherence in Vision Transformers	22
C.3 Comparisons with Monolithic Vision-Language Models	22
D Training Details of Experiments	23
D.1 Architectural Details	23
D.2 Self-supervised Pretraining	23
D.3 End-to-end Finetuning for Classification	23
D.4 Training for Fine-grained Visual Recognition	24
D.5 Computational Resources	24
E Details of the Used Datasets	24
F Limitations	26
G Societal Impacts	26

A More Visualizations with Attention Entropies

In Sections 4 and 5, we experimentally demonstrated the effectiveness of LUViT over the ViT baselines. Furthermore, we provided in-depth analysis regarding the background robustness properties of LUViT, where we demonstrated significant performance gains in Imagenet-9 [Xiao et al., 2020] with LUViT under adversarial backgrounds. Our empirical observations in Sections 4 and 5 were qualitatively grounded in the patterns we observe with the attention entropies of both LUViT and the ViT baseline. In particular, we showed that the foreground patches with LUViT exhibit significantly lower attention entropy compared to background patches, whereas the same distinction does not occur with the baseline ViT.

With the aim of solidifying these observations, we provide additional visualizations of the attention entropy patterns for both our LUViT and the baselines in this section. The visualizations and results presented in this section demonstrate that both the attention entropy patterns and the patch norms for LUViT provide significantly more salient visualizations compared to the ViT baseline (Section A.1), and that the observations made from the scatter plots in Section 5 generalize across all splits of the Imagenet-Segmentation benchmark (Section A.2).

A.1 Image-level Attention Entropy Visualizations

Here, we provide further details and image-level visualizations of attention entropy patterns along with the norms of the patches of both LUViT and our MAE pre-trained ViT baselines in Figure 3. Attention entropy patterns have been utilized in the context of neural network robustness in earlier

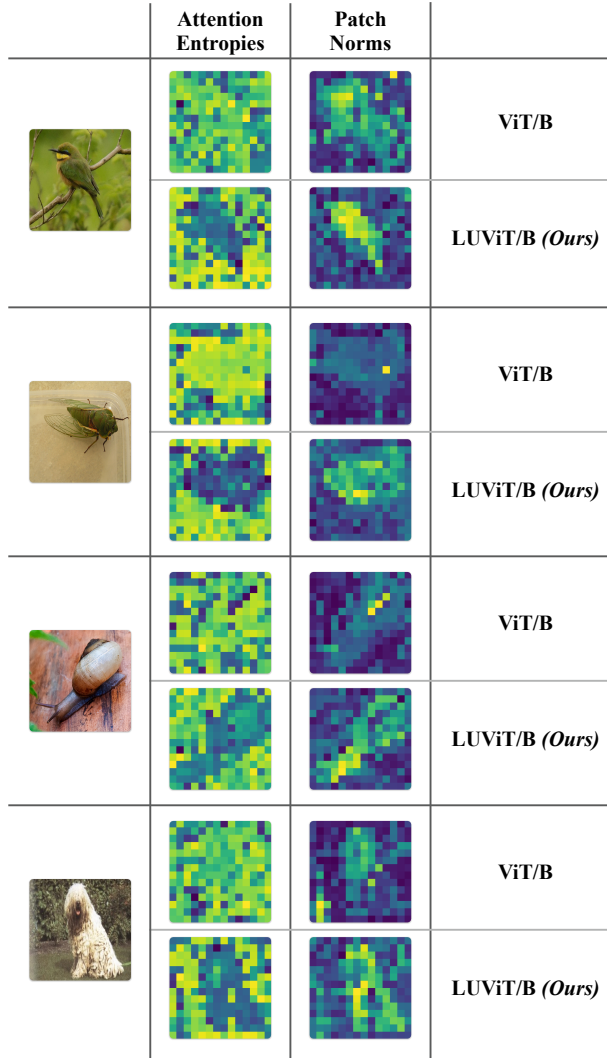


Figure 3: Visualized attention entropies and patch norms of both LUViT/B and the MAE pre-trained ViT/B baseline. LUViT/B simultaneously exhibits lower attention entropies and higher patch norms for foreground regions across all images compared to the ViT/B baseline, implying more focused attention patterns on these regions resulting in improved saliency in patch features. These results provide qualitative support to the background robustness behavior of LUViT/B over the ViT/B baseline. The brighter colors highlight patches with high attention entropy for the “**Attention Entropies**” column and the patches with higher norm for the “**Patch Norms**” column.

works [Guo et al., 2023, Zhang et al., 2024]. In these works, they provided litmus tests for measuring how focused the attention patterns of particular models are and how they relate to model robustness.

As stated in Section 5, we quantify the attention entropies through taking the post-softmax entropy of each row of the attention matrix, where each row corresponds to a spatial location, i.e., a patch, of the feature map, following the previous works using attention entropies [Zhai et al., 2023a].

Formally, denoting the input as $X \in \mathbb{R}^{T \times d}$, and the query and key projection matrices as $W_Q \in \mathbb{R}^{d \times d_k}, W_K \in \mathbb{R}^{d \times d_k}$, the attention weights are given by:

$$A = \text{softmax} \left[\frac{W_Q \cdot W_K^T}{\sqrt{d}} \right], \quad (3)$$

with the corresponding row-wise attention entropies then given by:

$$\mathcal{H}(A_i) = - \sum_{j=1}^T A_{i,j} \log(A_{i,j}). \quad (4)$$

Notably, we also average the attention entropies for each attention head, following the methodology of Zhai et al. [2023a]. Finally, to further supplement our visualizations, we additionally extract the L2 norms of each patch and visualize it alongside the attention entropy patterns.

Following this quantification process, we visualize the attention entropies along with the patch norms of both the final ViT block for both LUViT and the MAE pre-trained ViT baseline after finetuning on Imagenet-1K [Deng et al., 2009] in Figure 3. For Figure 3, we perform a per-image normalization for both the patch norms and attention entropies to achieve more interpretable visualizations. This corresponds to performing the normalizations based on the lowest and highest attention entropy score or token norm value for each feature map separately, and follows the normalization strategy used for visualizations in Pang et al. [2023].

As it can be seen in Figure 3, LUViT exhibits much lower attention entropies for the patches belonging to foreground regions compared to ViT/B, providing further qualitative support for our observations in Section 5. Simultaneously, the patch norms are more salient and achieve better coverage of foreground regions for LUViT compared to ViT/B. This behavior is specifically important, since we are utilizing average pooling instead of relying on the [CLS] token, following the default implementation in the official MAE codebase. We refer the reader to Section D.3 for more details on the classification pipeline of LUViT and the baselines.

A.2 Additional Attention Entropy Scatter Plots

In Section 5, we presented the attention entropy scatter plots for the Imagenet-Segmentation-300 validation set [Gao et al., 2022]. Here, we additionally present the scatter plots for the other two Imagenet-Segmentation variants [Gao et al., 2022], namely for Imagenet-Segmentation-50 validation set in Figure 4 and for Imagenet-Segmentation-919 validation set in Figure 5. Similar to the plots in Section 5, each point in Figures 4 and 5 correspond to the average attention entropy for each image where the y-axis highlights the average attention entropy for the foreground patches whereas the x-axis highlights the average attention entropy for the background patches.

These results closely mirror those in Section 5, where again a very clear distinction emerges between the average attention entropies for the background and foreground regions for our LUViT/B. On the other hand, the attention entropies are mostly the same for all regions of the MAE pretrained ViT/B baseline, regardless of whether they belong to a highly informative foreground region or not.

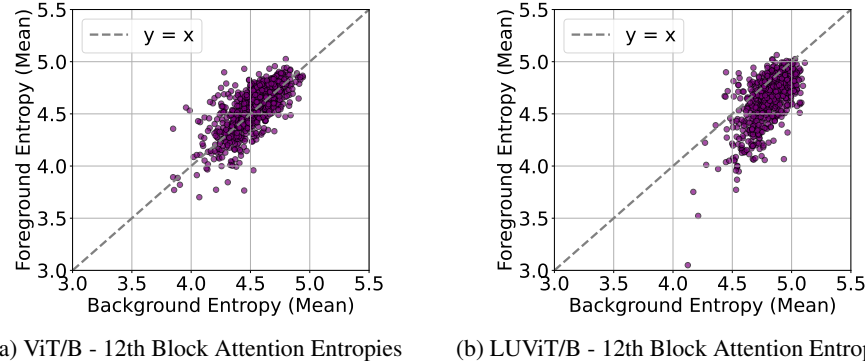
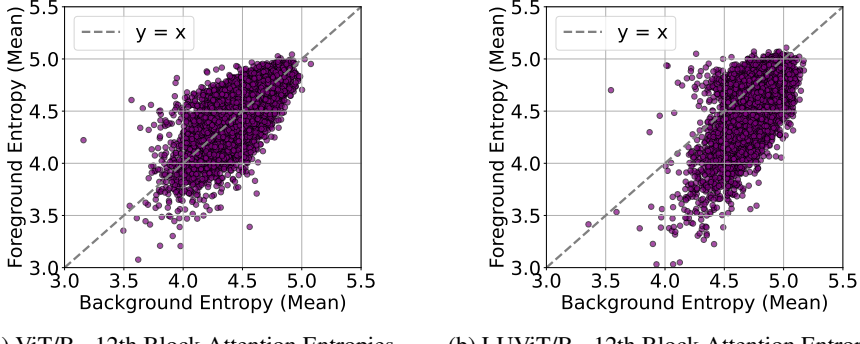


Figure 4: Comparison of the image-level average foreground attention entropies vs the image-level average background attention entropies of (a) MAE ViT/B baseline and (b) our LUViT/B model. Each point in the plots corresponds to an image on Imagenet-S-50 dataset [Gao et al., 2022]. LUViT’s average attention entropies are higher for background regions compared to foreground regions for 84% of the images. However, ViT/B’s average attention entropies are higher for background regions compared to foreground regions for only 42% of the images.



(a) ViT/B - 12th Block Attention Entropies (b) LUViT/B - 12th Block Attention Entropies

Figure 5: Comparison of the image-level average foreground attention entropies vs the image-level average background attention entropies of (a) MAE ViT/B baseline and (b) our LUViT/B model. Each point in the plots corresponds to an image on Imagenet-S-919 dataset [Gao et al., 2022]. LUViT’s average attention entropies are higher for background regions compared to foreground regions for 83% of the images. However, ViT/B’s average attention entropies are higher for background regions compared to foreground regions for only 44% of the images.

B Additional Experimental Results

In this section, we present additional experimental results to complement our analyses in Sections 4 and 5. In particular, we report error bars for the Imagenet-1K results presented in Table 1 in Section B.1, and additional results of performing LoRA adaptation of the LLM block in a supervised-only setting in Section B.2. Finally, we highlight the high quality of the attention maps of LUViT in the Imagenet-Segmentation dataset [Gao et al., 2022] in Section B.3.

B.1 Error Bars for Imagenet-1K Experiments

In Section 4, we have already demonstrated the effectiveness on both image classification and object detection. In Tables 1, 3 and 5, we reported the results after finetuning both our models and the baselines we reproduced with the random seed 0, directly adhering to the conventions of our baselines [He et al., 2022, Pang et al., 2023].

However, irrespective of the convention, the choice of random seed values has been shown to have nontrivial impacts on the end performance in the literature [Picard, 2021]. Therefore, to provide a fairer comparison, we trained both LUViT, MAE pretrained ViT/B baseline and the MAE pretrained ViT/B+MLP-L from Table 1 with 10 different random seeds in the range [0, 9], and report the results in Figure B.1.

The results in Table 1 show that the performance of LUViT/B provides remains consistently higher compared to either of the baselines. In particular, while ViT/B+MLP-L and ViT/B have nearly the identical accuracy, LUViT/ B has a mean higher than ViT/B+MLP-L and ViT/B by respectively 0.3% and 0.4%, closely mirroring the results presented in Table 1. Importantly, the 99% confidence intervals, denoted by the arrows at the bottom and top of the error bars, do not intersect between LUViT/B and the two baselines, further solidifying the significance of our performance gains.

B.2 Adapting the LLM Under Supervised-only Training

In Section 4, we demonstrated the effectiveness of employing Masked Auto-Encoding (MAE) to pre-train the ViT for richer visual representations, while concurrently training Low-Rank Adaptation (LoRA) layers within the LLM block using the same MAE objective.

Following our results and ablations in Section 5, a natural question may arise regarding how well a concurrent training strategy of Low-Rank Adaptation (LoRA) layers, and the ViT could work *without* the critical MAE pretraining phase. In this section, we investigate this question by including Low-Rank Adaptation (LoRA) layers on top of the architecture proposed in Pang et al. [2023] in a supervised-only setting.

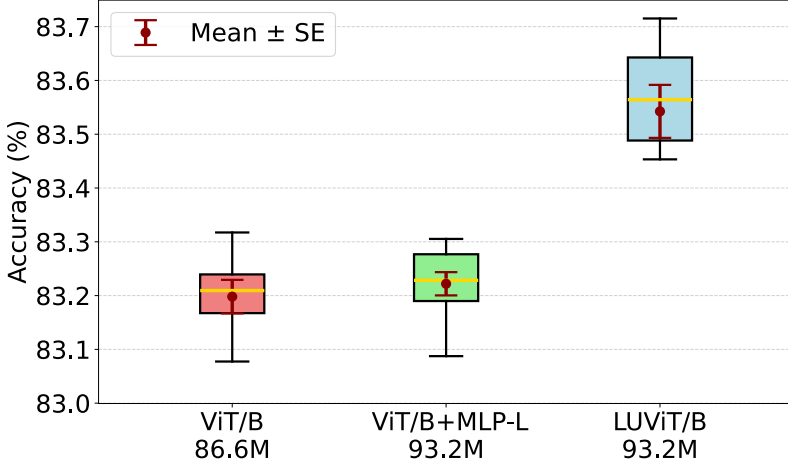


Figure 6: Top-1 accuracy bars along with the means and the standard error ranges of MAE pretrained ViT/B, MAE pretrained ViT/B+MLP-L and LUViT/B, reported after training with 10 random seeds in the range $[0, 9]$. Each models’ number of trainable parameters is stated respectively under their name. While the ViT/B+MLP-L results are similar to the ViT/B results, LUViT/B shows significantly better performance compared to either of the baselines, showing that the performance gains remain significant and are not a mere result of the additional trainable parameters.

The results of both our reproduction of Pang et al. [2023]’s model and its LoRA-adapted version is presented in Table 6. For Table 6, we train both Pang et al. [2023]’s LM1+ViT/B and its LoRA-adapted version in a supervised-only setting on Imagenet-1K with three different random seeds, $(0, 1, 2)$, while adhering to all training settings in Pang et al. [2023]. Furthermore, we directly utilize their code-base ², and merely inject trainable LoRA layers to its LLM block, similar to the methodology of LUViT presented in Sections 3 and 4. Finally, we report the average accuracy across the seeds with the accompanying standard error values, i.e. the standard deviation of the accuracy values divided by the number of different seeds.

From Table 6 we observe that the LoRA version achieves a slightly improved performance compared to the LM1+ViT/B. Concretely, the LoRA-adapted version of Pang et al. [2023]’s LM1+ViT/B has a $+0.12\%$ better accuracy compared to the completely frozen LM1+ViT/B. These results highlight that implying LoRA could potentially address the training instabilities that arise when directly finetuning the LLM block, even though the performance improvements are much less pronounced compared to LUViT’s improvements over the MAE ViT/B baselines.

Table 6: Adapting the LLM block in the ViT of Pang et al. [2023] with a supervised-only training regime. Each reported value is an average of three training runs with three seeds, $(0, 1, 2)$, and the subscript \pm denotes the standard error for each setting. Note that we report two significant digits in the decimal for highlighting the effect of standard errors in contrast with other tables. **Bold** denotes the best result while underline denotes second best for each setting.

Model	Average Accuracy
ViT/B+LLaMA	80.51 ± 0.07
+LoRA	80.63 ± 0.09

B.3 Additional Results on Imagenet-Segmentation Benchmark

In this section, following up from the qualitative observations with respect to token norms in Figure 3, we provide additional quantitative evidence that LUViT forms more salient patch features compared to the MAE pretrained ViT baseline. In particular, we compare the binary mask IoUs of the patch

²<https://github.com/zqipang/LM4VisualEncoding>

Table 7: Mask IoUs of the final ViT block for each model with respect to the Imagenet-Segmentation [Gao et al., 2022] segmentation annotations. Frequency column shows the results when the frequency component of the token features are used for obtaining the binary masks whereas the magnitude column shows the results when the magnitude component is used. **Bold** denotes the best result while underline denotes second best for each setting.

Model	INS-50		INS-300		INS-919	
	Frequency	Magnitude	Frequency	Magnitude	Frequency	Magnitude
MAE ViT/B	39.8	42.3	40.9	42.8	40.8	42.8
LUViT/B (<i>Ours</i>)	41.3	43.8	42.3	43.5	42.1	43.3
	<u>+1.5</u>	<u>+1.5</u>	<u>+1.4</u>	<u>+0.7</u>	<u>+1.3</u>	<u>+0.5</u>

features with respect to the ground truth segmentation masks presented in all three of the Imagenet-Segmentation splits [Gao et al., 2022] in Table 7, following the methodology of Pang et al. [2023].

In Pang et al. [2023], the authors leveraged a method to extract **magnitude** and **frequency** components from token features to generate pseudo-masks. Specifically, the magnitude component is obtained by taking the L2 norm of each token feature vector after centering, while the frequency component is obtained by taking the norm of the difference between the angle of a token feature vector and the average angle across all tokens in the same input, following a Fast Fourier Transform (FFT) [Pang et al., 2023].

Once these components are extracted for each token, binary pseudo-masks are created by applying a fixed threshold to either the magnitude or frequency values, assigning a binary label to each patch accordingly. This fixed threshold is determined empirically and individually for each component of each model, following the approach of Pang et al. [2023]. Finally, Pang et al. [2023] downsample the ground-truth segmentation masks in the ImageNet-Segmentation-50 dataset [Gao et al., 2022] to match the resolution of the model’s feature map. A cell in the downsampled mask is assigned a value of 1 if it overlaps with the original high-resolution mask. Concretely, this resolution is 14^2 for a ViT/B with patch size set to 16, with 224^2 resolution for images of Imagenet [Deng et al., 2009]. For more details regarding the frequency and magnitude components or the mask IoU measures, we refer the reader to the Appendix A.3 and Appendix A.5 of Pang et al. [2023].

As evidenced in Table 7, LUViT has a higher IoU not only across all three subsets of the Imagenet-Segmentation benchmark, but also with *both* of the frequency and magnitude components. Notably, the average improvement in terms of IoU gains for the frequency component of LUViT compared to the ViT/B is $+1.4$, while for the magnitude component of LUViT compared to the ViT/B is $+0.9$. These results further solidify the quantitative and qualitative analyses provided in Section 5 of the main work, while also grounding our qualitative observations in Section A.

C Further Discussions on Related Works

In this section, we discuss the closely related works to our work in more detail while highlighting the key differences, similarities and orthonogal directions between them and our LUViT framework.

C.1 Information Filtering Hypothesis

An important contribution of Pang et al. [2023] was the introduction of the *information filtering hypothesis*. Information filtering hypothesis was proposed as a potential explanation towards how a frozen LLM block could enhance the visual features for visual recognition tasks. Particularly, Pang et al. [2023] first follows from the DeiT [Touvron et al., 2021] family of models and perform classification based on the [CLS] token. Then, the authors made the claim that to achieve a better performance compared to the vanilla ViT/B, either the attention weights should be improving or the informative tokens should be getting amplified by the LLM block.

Formally, denoting the set of visual tokens with $v \in V$, attention weights of the final ViT block with w_v , the processed visual token v by the first linear layer following the ViT block as $M_L^1(z[v]) = z_v^1[v]$ and the the processed [CLS] token following the LLM block with $z'_{[CLS]}$, the hypothesis proposes the

following correlation:

$$z'_{[\text{CLS}]} \propto \sum_{v \in V} w_v (M_L^2 \cdot M_{LLM} \cdot z_v^1[v]), \quad (5)$$

with the assumption that the $M_L^2 \cdot M_{LLM} \cdot M_L^1$ is a linear projection.

However, Pang et al. [2023] made the qualitative observation that the attention weights, w_v , were noisy, thus concluding that the $M_L^2 \cdot M_{LLM}$ projection must be amplifying the most informative tokens.

While LUViT differs from Pang et al. [2023]’s frozen-LLM-appended ViTs in several key architectural and training-related details, our work also leverages the pretrained LLM representations to improve discriminative visual recognition asks. In addition, as we have also discussed in Section 5 and Section A, LUViT exhibits strong robustness against adversarial backgrounds compared to the baselines, an potential consequence of the information filtering hypothesis. Coupled with our attention entropy observations, analyses we present in Sections 5 and A can be thought in a similar spirit with the information filtering hypothesis where we provide complementary discussions.

C.2 Pretrained LLM Layers and Gradient Coherence in Vision Transformers

Another recent work investigating the underlying mechanisms behind how a frozen LLM block improves the visual recognition performance is proposed by Bai et al. [2025], where the authors approach from a gradient dynamics perspective.

In particular, Bai et al. [2025] broadly borrowed the architecture of Pang et al. [2023] and demonstrated that the gradient flow from different samples towards the weights of the model are more aligned in the presence of the frozen LLM block. The authors quantified this alignment through demonstrating improved gradient-signal-to-noise ratio (GSNR) under the presence of the LLM block. Notably, GSNR for a given parameter is the ratio between the squared expected value and the variance of the its gradient. A high GSNR is also tied with improved generalization for machine learning models [Liu et al., 2020, Michalkiewicz et al., 2023], and thus is a desirable property.

Bai et al. [2025] also showed that this effect is more pronounced towards layers closer to the LLM block, and that the similar representations between the ViT blocks and the LLM block could be indicative of improvements. Following up from this observation and taking inspirations from Tiwari and Shenoy [2023], Bai et al. [2025] then proposes an auxiliary training objective with the aim of removing the additional inference costs incurred by the LLM block. This auxiliary training objective distills the representations of the frozen-LLM-appended ViT to a vanilla ViT through a similarity loss in-between [Hinton et al., 2015].

Bai et al. [2025]’s work thus presents an orthogonal direction, and a potentially interesting future work for our work. Particularly, their auxiliary loss could be combined with our LUViT as the teacher model for distilling the vanilla ViT, as LUViT has stronger visual recognition performance compared to the baseline teacher models utilized in Bai et al. [2025].

C.3 Comparisons with Monolithic Vision-Language Models

A novel branch of works which are architecturally related to our work are foundation vision-language models aiming to contain both the vision and language modalities inside of a large monolithic transformer [Diao et al., 2024, 2025, Wang et al., 2025, Luo et al., 2024, Bavishi et al., 2023, Chen et al., 2024c]. These works are differ from other *encoder-decoder* [Li et al., 2022b, Liu et al., 2023, Li et al., 2023, Yu et al., 2022, Wan et al., 2024] or *two-tower encoder* [Radford et al., 2021, Tschannen et al., 2025, Zhai et al., 2023b] alternatives, where they enforce varying degrees of intra-block parameter sharing between the transformers for each modality. To exemplify, while Fuyu [Chen et al., 2024c], EVEv1 [Diao et al., 2024] all share the majority of the Transformer components, EVEv2 [Diao et al., 2025] only shares the self-attention block while having modality-specific layer norm (LN) [Ba et al., 2016] and MLP blocks inside each transformer.

While the monolithic vision-language models share some similarities with our work, they also differ in several key aspects. Namely, while our goal is to achieve stronger *discriminative* visual performance, these works mainly target generative domains, such as as visual question answering (VQA) [Goyal et al., 2017a] or image captioning [Chen et al., 2015].

In addition, all of the monolithic vision-language model works [Diao et al., 2024, 2025, Wang et al., 2025, Luo et al., 2024, Bavishi et al., 2023, Chen et al., 2024c] involve jointly training both the language and vision-related components on vast amounts of multi-modal data in multiple training stages with multiple objectives. In our work we merely adapt our LLM block with simple and cost-effective LoRA layers with a unified MAE objective without requiring any language-specific inputs or additional objectives, thereby achieving strong unimodal performance without extensive multimodal training.

D Training Details of Experiments

In this section, we describe the architectural details, hyperparameter settings and other training details that we adhered to throughout this work.

D.1 Architectural Details

Throughout our experiments, we utilize the ViT/B as our encoder from Dosovitskiy et al. [2020], which consists of 12 Transformer [Vaswani et al., 2017] blocks and has a hidden size of 768. In addition, for LUViT, we always utilize the 32nd (i.e the final) Transformer [Vaswani et al., 2017] block of the smallest LLaMA 1 [Touvron et al., 2023a] model with 7 billion parameters, which has a hidden size of 4096. We choose this block of LLaMA 1 following its success in similar works [Lai et al., 2024, Pang et al., 2023, Bai et al., 2025]. There are two additional linear projections *without* any non-linearities or additional activations around the LLaMA 1 block to allow matching the hidden dimensions of the ViT and the LLaMA 1.

During the pretraining stage, for both LUViT and our baselines, we additionally employ a lightweight Transformer [Vaswani et al., 2017] decoder, which consists of 8 blocks and has a hidden size of 512. The design of both the ViT/B encoder and the lightweight decoder closely mirror the original MAE design with no changes with the exception of the LLaMA 1 block and the linear projections around it.

Finally, the additional capacity baselines in Section 4 all have additional linear projection layers at the head, analogously with where they are placed in LUViT. For the ViT/B+MLP-L baseline, this corresponds to two linear projections, respectively with dimensions 768x4267 and 4267x768 and for the ViT/B+MLP-P baseline, this corresponds to two linear projections, respectively with dimensions 768x4096 and 4096x768.

D.2 Self-supervised Pretraining

For all of our self-supervised pretraining experiments, we directly adhere to all of the settings presented in the original MAE work [He et al., 2022], while training both our models and the baselines for 800 epochs.

Namely, this corresponds to having a batch size of 4096, base learning rate of 1.5e-04, with cosine annealing scheduling [Loshchilov and Hutter, 2016]. In addition, we used the AdamW optimizer [Kingma, 2014, Loshchilov and Hutter, 2017] with $\beta_1 = 0.90$ and $\beta_2 = 0.95$ [Chen et al., 2020b], coupled with 40 warm-up epochs [Goyal et al., 2017b] and a weight decay of 0.05. Finally, we also apply a random resized crop augmentation, utilized a random masking ratio of 75% for masking the encoder inputs, and a normalized pixel version of mean squared error (MSE) between the reconstructed and the ground truth images as the objective.

D.3 End-to-end Finetuning for Classification

Analogously with Section D.2, we directly adhere to all of the settings presented in the original MAE work [He et al., 2022]. Namely, this corresponds to having a batch size of 1024, learning rate of 1.e-03, with cosine annealing scheduling [Loshchilov and Hutter, 2016]. In addition, we used the AdamW optimizer [Kingma, 2014, Loshchilov and Hutter, 2017] with $\beta_1 = 0.90$ and $\beta_2 = 0.999$ [Chen et al., 2020b], coupled with 5 warm-up epochs [Goyal et al., 2017b] and a weight decay of 0.05. Differing from the pretraining stage, here we have a layer-wise learning rate decay value of 0.75 [Bao et al., 2021, Clark et al., 2020], label smoothing of 0.1 [Szegedy et al., 2016] and a drop path rate of 0.1 [Huang et al., 2016]. Finally, we also applied *mixup* [Zhang et al., 2017] with 0.8, *cutmix* Yun et al. [2019] with 1.0, and *Randaugment* with (9, 0.5) [Cubuk et al., 2020].

Notably, we utilize average pooling setting instead of relying on the [CLS] token for performing classification. We do so, following the official MAE Github repository’s³ report of potential instabilities in the loss values⁴ when the [CLS] token was used with Pytorch [Paszke, 2019].

D.4 Training for Fine-grained Visual Recognition

Our fine-grained visual recognition experiments mostly follow from the ViTDet framework [Li et al., 2022a], which is a competitive fine-grained visual recognition framework achieving competitive results with plain ViT backbones [Dosovitskiy et al., 2020] with respect to previously-stronger hierarchical counterparts, such as the Swin Transformer [Liu et al., 2021]. ViTDet framework involves taking an MAE pretrained plain ViT backbone, a following simple feature pyramid structure Lin et al. [2017] and a Mask R-CNN [He et al., 2017] as the final detection/segmentation head. Notably, achieving competitive fine-grained visual recognition results is very hard with supervised-only ViT backbones, with neither of Imagenet-1K nor Imagenet-22K supervised-pretrained ViT/B models achieving better results than a randomly initialized ViT/B, further highlighting the necessity of self-supervised pretraining for achieving strong fine-grained visual recognition.

Finally, the entire model, with the notable exception of the LLM block that we always keep frozen and merely adapt through the LoRA layers, including the ViT/LUViT backbones, is trained jointly on the COCO training set [Lin et al., 2014], with a batch size of 64, a learning rate of $1.5e-04$, weight decay of 0.1, drop path rate of 0.1 and for 100 epochs. For both our baselines and LUViT, we directly adhere to the settings of Li et al. [2022a], and do not change any hyperparameters. We implemented our LUViT/B ViTDet and benchmarked both LUViT and our baselines on the mmdetection library [Chen et al., 2019].

D.5 Computational Resources

For all of the aforementioned experiments, we ran our experiments on 32 NVIDIA A100 GPUs. For MAE pretraining described in Section D.2, both the LUViT and the baseline experiments take approximately 30 hours. For both the end-to-end finetuning for classification and the fine-grained visual recognition training experiments, both LUViT and the baseline experiments take approximately 24 hours.

E Details of the Used Datasets

In this section, we provide the details of the datasets we used for our experiments and other quantitative analyses, while clarifying the exact splits and settings we report our results on.

Imagenet-1K. Imagenet-1K [Deng et al., 2009] consists of $1.2M$ training and $50K$ validation images, belonging to 1000 different classes. Following the conventional approach [He et al., 2016, Dosovitskiy et al., 2020], we used the resized (224^2) images for both training and evaluation. We performed the MAE pretraining exclusively on Imagenet-1K training set, for all of our classification and fine-grained visual recognition experiments, following our baselines [He et al., 2022, Li et al., 2022a].

Imagenet-9. Imagenet-9 [Xiao et al., 2020] consists of images of the 9 super-classes from the original Imagenet-1K validation set [Deng et al., 2009], and aims to measure the background over-reliance of deep learning models in an evaluation-only setting. In particular, Imagenet-9 has contains numerous splits, such as the *original*, *mixed random*, *mixed same*, and *mixed next*. The first of these splits, *original* consists of the unaltered images belonging to the 9 super-classes, with their original backgrounds. On the other hand, *mixed random*, *mixed same*, and *mixed next* consist of images with altered backgrounds. For *mixed random*, the background of each image is replaced with the background of another image from a random super-class, for *mixed next*, the background of each image is replaced with the background of another image from the next super-class ordered with respect to their numerical IDs, and for *mixed same* the background of each image is replaced with the background of another image from the same super-class.

³<https://github.com/facebookresearch/mae/tree/main>

⁴<https://github.com/facebookresearch/mae/blob/main/FINETUNE.md>

In Imagenet-9 [Xiao et al., 2020], while it is desirable to obtain high performance on the clean *original* set, it is crucial to obtain high performance on the splits with altered backgrounds for demonstrating the robustness of the models, thereby achieving a smaller *background accuracy gap*. Finally, for our evaluations, we utilized the *original* split for benchmarking the clean accuracy of the models in our work, while comparing it to the accuracies in *mixed random* and *mixed same* splits for measuring the background over-reliance of models.

Imagenet-Segmentation. Imagenet-Segmentation [Gao et al., 2022] consists of the images and associated high-quality segmentation masks of the original Imagenet-1K [Deng et al., 2009] images. It has 3 splits of different sizes, Imagenet-Segmentation-50 as the 50 class subset with 752 validation images, Imagenet-Segmentation-300 as the 300 class subset with 4K validation images, and Imagenet-Segmentation-919 as the 919 class subset with 12K validation images. Notably, the largest 919 split does not contain the images of non-segmentable 81 classes from the original Imagenet-1K splits [Gao et al., 2022]. We re-purpose this dataset in the same format as Pang et al. [2023], though including additional results and visualizations on the more challenging Imagenet-Segmentation-300 and Imagenet-Segmentation-919 instead of limiting the analyses to the limited Imagenet-Segmentation-50 split as in Pang et al. [2023].

Imagenet-C. Imagenet-C [Hendrycks and Dietterich, 2019] benchmark is an evaluation-only benchmark consists of synthetically corrupted images belonging to the Imagenet-1K validation [Deng et al., 2009] set. In particular, there are 15 benchmark corruptions, namely 4 noise corruptions (*gaussian noise, shot noise, impulse noise*), 4 weather-related corruptions (*snow, frost, fog, brightness*), 4 blurring corruptions (*defocus, glass, motion, zoom*) and 3 digital corruptions (*contrast, elastic transform, pixelate*). Furthermore, there are 4 additional corruptions, namely *gaussian blur, spatter, saturate, speckle noise*, bringing the total to 19. For each of these corruptions, there are 5 severity levels, with higher number indicating tougher corruptions. In our experiments, we report the average results on all of the aforementioned corruptions with all of their severities for a more comprehensive evaluation.

Imagenet-A. Imagenet-A [Hendrycks et al., 2021a] is an adversarially-designed benchmark consisting of images from Imagenet-1K validation set, where the majority of the Imagenet-1K-trained classifiers fail. Notably, it has 200 super-classes instead of the full 1000 classes of the Imagenet-1K benchmark, where the super-classes were explicitly constructed in a way that confusing them would be beyond a simple confusion of similar classes.

Imagenet-SK. Imagenet-SK [Wang et al., 2019] consists of 50K images of sketches of Imagenet-1K classes, 50 for each of the 1000 classes of the Imagenet-1K validation set. Notably, images of Imagenet-SK are *black and white* sketches, posing a challenge due to their lack of texture and color information.

Imagenet-V2. Imagenet-V2 [Recht et al., 2019] is a benchmark proposed to measure the broader generalization capabilities of Imagenet-1K-trained models. It also has samples for the same 1000 classes of the Imagenet-1K, though with specifically curated examples where the majority of the Imagenet-1K-trained classifiers tend to fail. Among its different variants, we utilized the *matched frequency* version, as it is proposed to be the default setting in Recht et al. [2019].

Imagenet-R. Imagenet-R [Hendrycks et al., 2021b] is a 30K image domain-generalization benchmark for Imagenet-1K-trained classifiers. It contains “*renditions*” of images belonging to Imagenet-1K classes, in the form of images of sculptures or paintings, with drastically different textures, and other often-helpful image-level statistics.

MS COCO. MS COCO [Lin et al., 2014] is an object detection and instance segmentation benchmark for benchmarking fine-grained visual recognition capabilities of deep learning models. Among its variants, we train both LUViT/B with ViTDet [Li et al., 2022a] and ViT/B with ViTDet [Li et al., 2022a] models on COCO2017 training set and report our results on the COCO2017 validation set, following the common practice [Li et al., 2022a, Carion et al., 2020, He et al., 2017].

F Limitations

Even though LUViT benefits from the combined powers of self-supervised learning with MAE and the LoRA-adapted pretrained LLM representations for discriminative computer vision tasks, it also inherits the drawbacks of these works. First, while LUViT does not introduce a significant training overhead over the ViT baselines, the computational costs of MAE pretraining is still substantial, even though it is drastically cheaper compared to alternative self-supervised learning methods [Oquab et al., 2023, Caron et al., 2021]. In addition, the two-stage training nature of our framework can be undesirable for the practitioners of downstream applications. On the other hand, the addition of the LLM block inevitably introduces an increase in the inference time over our vanilla ViT baselines, which may limit its usage on downstream tasks requiring real-time processing.

G Societal Impacts

As described in Section D.5, LUViT relies on GPU-accelerated training to achieve an effective training time. Associated with the negative impact of GPUs on environment [Lacoste et al., 2019], this can have undesirable effects. Similar to any other computer vision model, our models can have associated bias or fairness concerns owing to their pre-training data. On the other hand, significantly improved robustness properties with our models can be desirable on a plethora of downstream applications, potentially having a positive impact.